JOURNAL OF CATALYSIS 155, 131–140 (1995)

Iridium Clusters in KLTL Zeolite: Structure and Catalytic Selectivity for *n*-Hexane Aromatization

N. D. Triantafillou,* J. T. Miller,† and B. C. Gates*,‡,[1]

*Center for Catalytic Science and Technology, Department of Chemical Engineering, University of Delaware, Newark, Delaware 19716; †Amoco Oil Company, Research and Development Department, P.O. Box 3011, Naperville, Illinois 60566; and ‡Department of Chemical Engineering and Materials Science, University of California, Davis, California 95616

Received October 13, 1994; revised April 11, 1995

Catalysts consisting of Ir clusters in zeolite KLTL were prepared by reduction of $[Ir(NH_3)_5Cl]Cl_2$ in the zeolite with H_2 at temperatures 300 or 500°C. The catalysts were tested for reactions of *n*-hexane and H_2 at 400, 440, and 480°C and were characterized by temperature-programmed reduction, hydrogen chemisorption, transmission electron microscopy, infrared spectroscopy of adsorbed CO, and extended X-ray absorption fine structure spectroscopy. The clusters consist of 4 to 6 Ir atoms on average and are sufficiently small to reside within the pores of the zeolite. The infrared spectra characteristic of terminal CO suggest that the support environment is slightly basic and that the Ir clusters are electron rich relative to the bulk metal. Notwithstanding the small cluster size, the support basicity, and the confining geometry of the LTL zeolite pore structure, the catalytic performance is similar to those of other Ir catalysts, with a poor selectivity for aromatization and a high selectivity for hydrogenolysis. These results are consistent with the inference that the principal requirements for selective naphtha aromatization catalysts are both a nonacidic support and a metal with a low hydrogenolysis activity, i.e., Pt.

INTRODUCTION

Pt clusters in basic LTL zeolite are active, stable, and selective catalysts for the dehydrocyclization of straight-chain paraffins to give aromatics (1–4). Research with these catalysts has led to the commercial development of a new naphtha reforming process for production of benzene for the petrochemical industry (5, 6).

Several explanations have been proposed for the exceptional performance of this catalyst, and the issues are still debated. There is general agreement that the dehydrocyclization is catalyzed by a single function, the Pt (2, 4, 7), and that the support must be nonacidic to prevent yield loss by acid-catalyzed isomerization and hydrocracking (2, 8). Several groups have demonstrated that the more basic the LTL support, the higher the aromatic selectivity of the catalyst. The interaction of the Pt clusters with the basic support is thought to result in an increase in the electron density of the Pt, leading to a modification of the adsorptive (9, 10) and catalytic (11–15) properties.

The zeolite support may influence the catalytic performance by affecting the steric environment of the clusters. According to one explanation (16), the one-dimensional pore structure of the LTL zeolite orients the reacting straight-chain paraffin parallel to the pore axis, thereby increasing the probability of terminal adsorption. Collimation effects have been demonstrated for ring opening of methylcyclopentane, whereby the methyl group is oriented parallel to the pore axis, increasing the selectivity to 3-methylpentane and *n*-hexane (17). Alternatively, cyclic adsorption of paraffins on the zeolite pore wall has been suggested to orient the reactant in a pseudocyclic conformation similar to the transition state required for aromatic formation (18).

However, the same group which proposed this cyclic adsorption model later ruled out the importance of spatial and adsorptive effects of the zeolite because catalytic selectivities similar to those observed for the zeolite-supported Pt clusters were also observed for Pt clusters supported on basic magnesia–alumina hydrotalcite clay (19–21). But the steric influence of the narrow zeolite pores has been proposed to inhibit deactivation of the Pt catalyst, presumably by restricting bimolecular reactions leading to carbon deposition; thus the high aromatic selectivity has been suggested to be characteristic of the clean Pt surface (22).

Because well-prepared catalysts incorporate extremely small Pt clusters (with approximately 6 atoms per cluster, on average), with almost no Pt outside the pores (7, 23, 24), the high benzene selectivity has alternatively been attributed to the low hydrogenolysis activity of Pt clusters smaller than about 1 nm (8). The small cavities characteristic of the LTL structure evidently favor small, stable Pt clusters.

[1] To whom correspondence should be addressed at the University of California.

0021-9517/95 $12.00

In summary, the role of the zeolite support in these catalysts is not yet well understood, and our objective was to prepare and investigate small clusters of another metal, Ir, in this support to determine whether small clusters of this metal in the zeolite would have a higher selectivity for dehydrocyclization than is associated with Ir, which typically has a high selectivity for hydrogenolysis and a low selectivity for dehydrocyclization. The catalyst was made from an iridium salt and characterized by extended X-ray absorption fine structure (EXAFS) spectroscopy, infrared spectroscopy of adsorbed CO, H_2 chemisorption, and transmission electron microscopy (TEM).

EXPERIMENTAL METHODS

Catalyst Preparation

$[Ir(NH_3)_5Cl]Cl_2$ was prepared according to published procedures (25). A solution of 3.1 g of $K_3[IrCl_6] \cdot 3H_2O$, 29 g of $(NH_4)_2CO_3$, and 20 g of NH_4Cl in water was refluxed under NH_3. The product was recrystallized and washed with aqueous solutions of HCl and then ethanol. Elemental analysis confirmed the synthesis.

The KLTL zeolite (Union Carbide) was washed with water until the pH of the wash solution was 9.5. The dried zeolite was calcined in air at 400°C and then crushed into a fine powder. $[Ir(NH_3)_5Cl]Cl_2$ (1 g) was dissolved in 40 ml of water by heating to 70°C, and the solution was added dropwise to 50.0 g of zeolite. Elemental analysis of the catalyst indicated that it contained 1.0 wt% Ir, 8.3 wt% Al, and 13.0 wt% K; the Si : Al atomic ratio of the zeolite was 3.6, and the K : Al atomic ratio was 1.08 [a value that has been shown to give good Pt/KLTL dehydrocyclization catalysts (7)]. The Ir/KLTL catalyst was reduced in flowing H_2 at 1 atm; the temperature was increased at 5°C/min from room temperature to either 300 or 500°C.

Catalytic Reactions

The conversion of *n*-hexane (Aldrich, 99.5%, with impurities of 0.4 wt% methylcyclopentane and 0.1 wt% 3-methylpentane) was conducted at 1 atm in a once-through Pyrex flow reactor at a temperature of 400, 440, or 480°C. H_2 (Matheson, 99.999%) and He (Matheson, 99.999%) were purified by flow through activated traps containing a 4 Å molecular sieve and Cu_2O. Catalyst (15 to 100 mg) was crushed to 150–180 μm particles and mixed with inert alundum particles in a volume ratio of 1 : 10. Prior to reaction, the catalyst was reduced in flowing H_2 by heating at 5°C/min to 500°C. After 1 h at 500°C, the catalyst was cooled to the reaction temperature. *n*-Hexane was fed by a syringe pump to a vaporization chamber heated to 73°C, where it was mixed with H_2 and He. The H_2, He, and *n*-hexane flow rates were adjusted to give an *n*-hexane partial pressure of 76 Torr and a H_2 : *n*-hexane molar ratio of 6. The reaction product vapors were analyzed with an on-line gas chromatograph equipped with a flame ionization detector and a 30 ft × $\frac{1}{8}$ in. 23% SP-1700/Chromosorb PAW packed column. At 480°C in the absence of catalyst, there was no measurable conversion of *n*-hexane.

Catalyst Characterization

Temperature-programmed reduction (TPR). Approximately 50 mg of Ir/KLTL was heated from 25 to 800°C at 5°C/min in 5% H_2 in N_2 flowing at 10 ml/min; the products were detected by a thermal conductivity detector.

Transmission electron microscopy. The electron microscope was a Philips 400T TEM operated at 120 kV. The Ir/KLTL catalyst was prereduced at 500°C, cooled to room temperature in H_2, and purged for 15 min with N_2 prior to exposure to air. The sample was ground to a fine powder, embedded in LR white resin, and sectioned with an ultramicrotome. Thin sections were mounted on copper grids and lightly coated with carbon.

Hydrogen chemisorption. Samples were crushed and screened to 60/100 mesh particles and reduced for 1 h in flowing H_2 at 1 atm and either 300 or 500°C. The reduced catalysts were evacuated at 300°C for 12 h at 10^{-5} Torr. Hydrogen adsorption measurements were made in conventional apparatus at pressures between 0 and 300 Torr. Measurements were also made for KLTL zeolite without Ir. Details are given in a thesis (26).

Infrared spectroscopy of adsorbed CO. Transmission infrared spectra of adsorbed CO (Matheson, 99.999%) were obtained with a Nicolet 510M spectrometer. Prereduced samples were pressed into semitransparent wafers in a N_2-filled glovebox and loaded into sealed cells with NaCl windows. The infrared cell could be heated with the sample in the presence of flowing gases or under vacuum. The reduced samples were exposed to 28 Torr of CO for 30 min, followed by evacuation of the cell (5×10^{-5} Torr) at room temperature. For samples exposed to flowing CO and treated at different temperatures, the spectra were obtained after purging with flowing He and cooling to 25°C.

EXAFS spectroscopy. Data were collected at beam line X-11A at the National Synchrotron Light Source at Brookhaven National Laboratory. The storage ring operated with an electron energy of 2.5 GeV and a current of 200–200 mA. The Si(111) monochromator was detuned by 30% to minimize higher harmonics in the X-ray beam. The samples were pressed into self-supporting wafers and placed into a controlled atmosphere cell. Data were

collected at the Ir L_{III} edge (11,215 eV) at liquid nitrogen temperature and in the presence of H_2 after reduction of the catalyst in flowing H_2 at either 300 or 500°C. The data were acquired in the transmission mode for 1 s per point in the range from 200 eV before the absorption edge to 30 eV beyond the absorption edge, for 2 s from 30 to 400 eV beyond the edge, and for 4 s at higher energies.

EXAFS data analysis (27). Experimentally determined phase shifts and backscattering amplitudes for Ir–Ir and Ir–O were obtained from EXAFS data for Pt foil and $Na_2Pt(OH)_6$, respectively. The data from two scans for each Ir/KLTL catalyst were averaged and analyzed with the Vaarkamp–Koningsberger University of Utrecht EXAFS data analysis software to estimate the parameters that characterize the high-Z (Ir) and low-Z (O) contributions by multiple-shell fitting in k space (k is the wave vector) and in r space (r is the distance from the absorbing atom, Ir). The different contributions in the EXAFS data were determined by applying the Koningsberger difference file technique to phase- and amplitude-corrected Fourier transforms (27). To avoid a significant underestimation of the contributions of either the low-Z or high-Z contributions, the fit parameters characterizing the Ir and O contributions were optimized with both k^1- and k^3-weighting. Once a close fit was obtained for the EXAFS parameters, N, $\Delta\sigma^2$, R, and ΔE_0 (where N is the coordination number, $\Delta\sigma^2$ the Debye–Waller factor, R the radial distance from the absorber to the backscatter atom, and ΔE_0 the inner potential correction) with k^1- and k^3-weighting, the fit was optimized by allowing a few of the parameters to be fitted while the rest of the parameters were held fixed.

RESULTS

Temperature-Programmed Reduction

The Ir-containing zeolite consumed H_2 in two stages, indicated by the peaks at about 270°C and about 290°C in the TPR spectrum (Fig. 1). The reduction of Ir was judged to be complete after 10 min at 300°C in flowing 10.4% H_2 in N_2. These results indicate that Ir(III) ions in the zeolite had been fully reduced to zerovalent Ir at treatment temperatures > 300°C.

H_2 Chemisorption

Extrapolation of the hydrogen adsorption isotherm to zero pressure resulted in a H/Ir value of 2.6 for both the catalyst reduced at 300°C and that reduced at 500°C. Similar hydrogen chemisorption results were obtained for highly dispersed Ir/alumina catalysts and were suggested to indicate formation of iridium hydride-like species (28). The quantity of hydrogen adsorbed by the KLTL support was approximately 5% of that observed for the supported Ir catalyst.

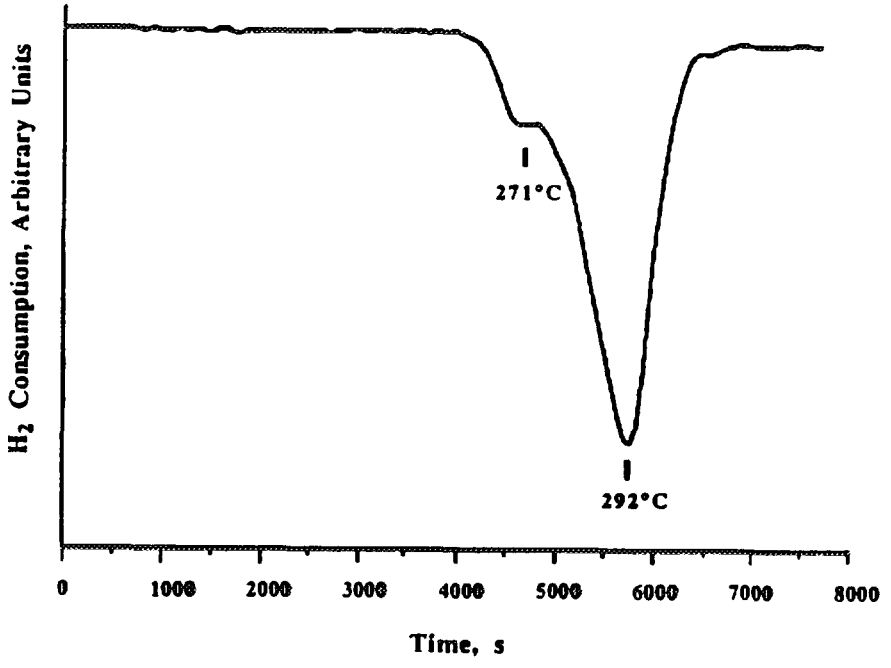

FIG. 1. Temperature-programmed reduction data indicating hydrogen consumption by the KLTL zeolite prepared from $[Ir(NH_3)_5Cl]Cl_2$.

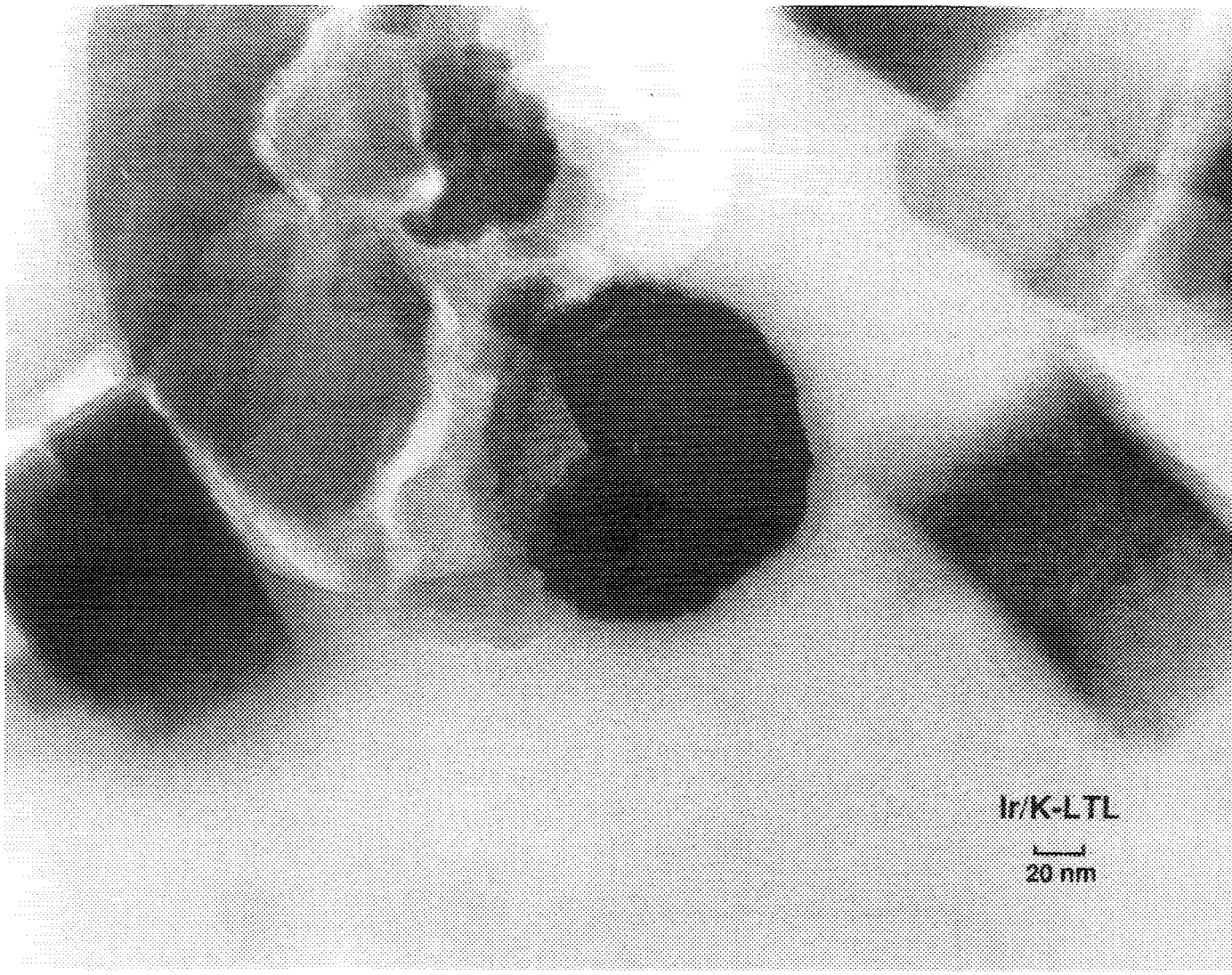

FIG. 2. Electron micrograph of KLTL zeolite prepared with $[Ir(NH_3)_5Cl]Cl_2$ after treatment in flowing H_2 at 500°C for 1 h. The Ir loading was 1.0 wt%.

Transmission Electron Microscopy

An electron micrograph Ir/KLTL reduced at 500°C is shown in Fig. 2. The KLTL zeolite crystals are cylindrical (23) and appear rounded or rectangular in shape, ranging in size from 0.03 to 0.5 μm. Lattice images, with a spacing of 1.66 nm, are normal to the channel direction in the rectangular particles. Few Ir clusters larger than about 2 nm are evident in the micrographs (Fig. 2). At high magnification, a few small Ir particles are visible between the lattice spacings; however, the majority of the Ir clusters are too small to be imaged with the microscope. Similar results (not shown) were obtained for the catalyst reduced at 300°C. The results suggest that after reduction at each temperature, the Ir was highly dispersed, and the cluters were small enough to be located inside the pores of the zeolite.

Infrared Spectroscopy of Adsorbed CO

The infrared spectrum of Ir/KLTL reduced at 300°C and exposed to 28 Torr CO (Fig. 3) is characterized by linearly bonded CO, with ν_{CO} bands at 2067s, 2036s, and 1986s cm^{-1} and a bridge-bonded CO with a ν_{CO} band at 1773 cm^{-1}. Exposure of the Ir/KLTL catalyst reduced at 300°C to CO at 1 atm and 50°C (Fig. 3B) resulted in a spectrum with ν_{CO} bands at 2065ssh, 2032s, 2004s, 1960m, and 1895w cm^{-1}. The spectrum of the catalyst reduced at 500°C and exposed to 28 Torr of CO was

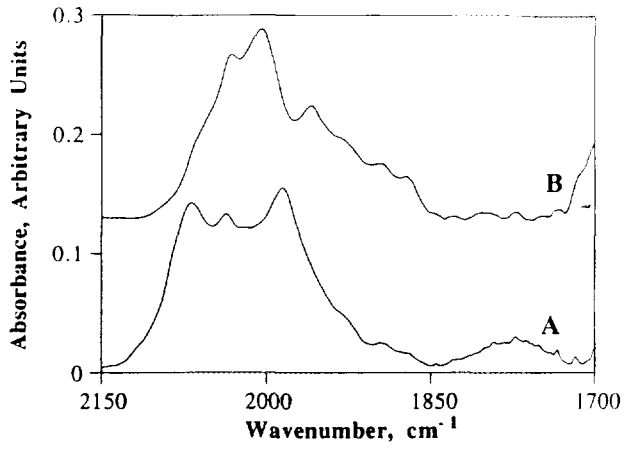

FIG. 3. Infrared spectra of chemisorbed CO on Ir/KLTL zeolites. (A) Sample that had been treated at 300°C in H_2 for 1 h, evacuated at 8×10^{-5} Torr, exposed to 28 Torr CO at 25°C, and evacuated at 5×10^{-5} Torr; (B) sample that had been treated at 300°C in H_2 for 1 h, treated in flowing CO at 1 atm and 50°C for 1 h, and purged with He at 25°C.

almost the same as that of the catalyst reduced at 300°C (e.g., Fig. 3A).

EXAFS Analysis

The raw EXAFS data for Ir/KLTL reduced at 300 and at 500°C are given in Fig. 4A. At low values of k, the amplitude of the EXAFS function is slightly greater for the catalyst reduced at 300°C than for that reduced at 500°C. In addition, there is a slight shift in the node positions in the range of k = 3–5 Å^{-1}. At high values of k, the amplitude is slightly greater for the catalyst reduced at 500°C. The normalized EXAFS functions are shown in Figs. 5A and 5C. Fourier transforms (not shown) of the EXAFS data show a slight increase in the amplitude of the Ir–Ir contribution at around 2.7 Å for Ir/KLTL reduced at 500°C relative to that reduced at 300°C. An additional scatterer besides Ir is evident as a separate peak near 1.8 Å (uncorrected). This peak is larger for the catalyst reduced at 300°C than for that reduced at 500°C.

Multiple shell fitting of the Fourier-filtered EXAFS spectrum (k^2-weighted, Δk: 3.64–11.68 Å^{-1}; Δr: 1.592–4.183 Å) of Ir/KLTL reduced at 300°C resulted in the identification of three significant contributions (Table 1): an Ir–Ir contribution at 2.70 Å with a coordination number of 3.2 (indicating ca. 4 Ir atoms/cluster), an Ir–O contribution at 2.18 Å with a coordination number of 1.2, and a second Ir–O contribution at 2.60 Å with a coordination number of 2.5. The number of parameters used to fit the data is 12, with approximately 14 degrees of freedom. This latter value was estimated from the Nyquist theorem (29), $n = (2\Delta k \Delta r/\pi) + 1$, where Δk and Δr, respectively,

TABLE 1

EXAFS Results Characterizing the KLTL Zeolite-Supported Iridium Clusters Prepared by the KLTL Zeolite with $[Ir(NH_3)_5Cl]Cl_2$ Followed by Flowing H_2 at 300°C and 1 atm for 1 h

Shell	N	R (Å)	$\Delta\sigma^2$ (Å^2)	ΔE_0 (eV)	EXAFS reference
Ir–Ir	3.2	2.70	0.0017	−0.45	Pt–Pt
Ir–O_s	1.2	2.18	0.0034	−4.68	Pt–O
Ir–O_l	2.5	2.60	0.0088	−0.47	Pt–O

Note. N, coordination number for absorber–backscatterer pair; R, radial absorber–backscatterer distance; $\Delta\sigma^2$, Debye–Waller factor (difference with respect to reference compound); ΔE_0, inner potential correction (correction of the edge position). Estimated precision: N, ±20% ($Ir–O_{support}$, ± 30%); R, ± 2% (Ir–Ir, ± 1%); $\Delta\sigma^2$, ± 30%; ΔE_0, ±10%. The subscripts s and l refer to short and long, respectively.

are the k and r ranges used in the forward and inverse Fourier transforms (Δk = 8.04 Å^{-1}; Δr = 2.59 Å).

Comparisons of the k^1- and k^3-weighted data and fit,

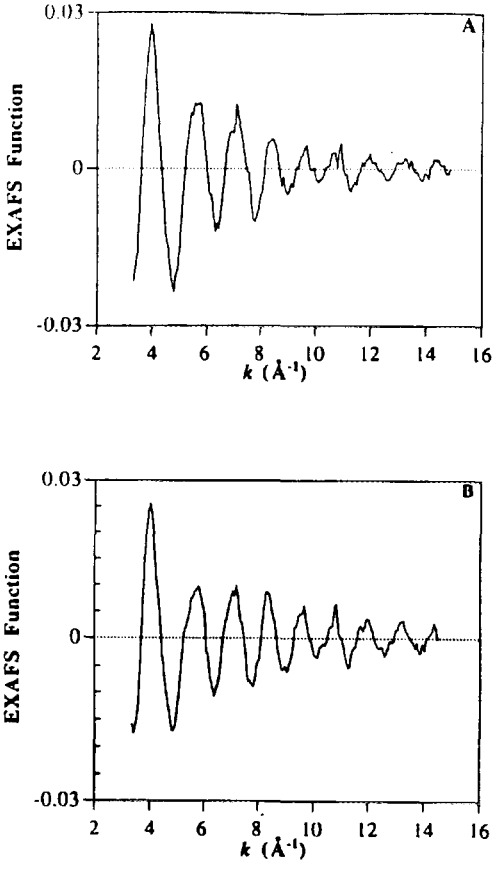

FIG. 4. Raw EXAFS data at the Ir L_{III} edge for samples of KLTL zeolite containing 1 wt% Ir after treatment (A) in H_2 at 300°C for 1 h and (B) in H_2 at 500°C for 1 h. Samples were scanned in the presence of H_2 at liquid N_2 temperature.

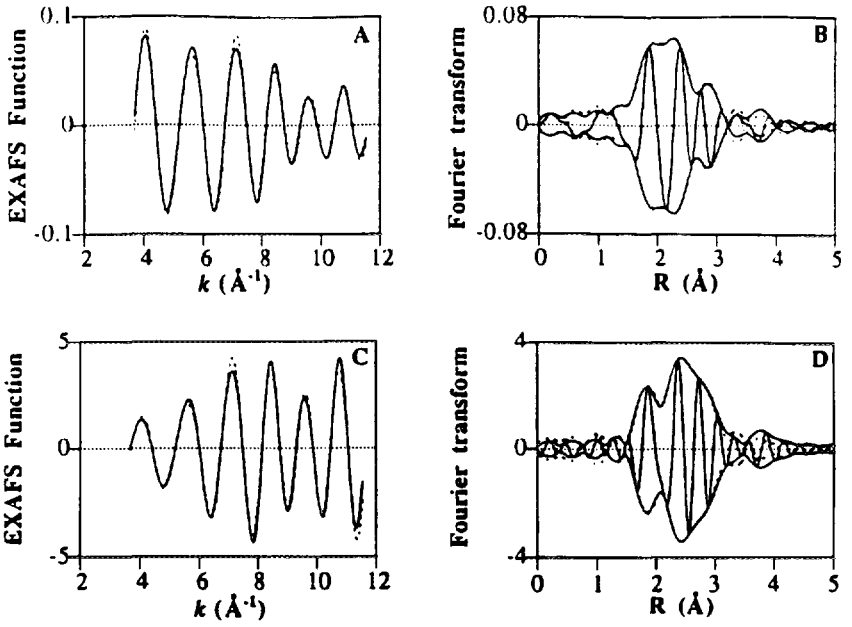

FIG. 5. Results of EXAFS analysis obtained with the best calculated coordination parameters characterizing supported Ir clusters prepared by treatment of KLTL zeolite prepared from $[Ir(NH_3)_5Cl]Cl_2$ treated at 300°C in flowing H_2 for 1 h. (A) Normalized EXAFS function (solid line) and sum of the calculated Ir–Ir + Ir–O_S + Ir–O_I contributions (dotted line) (k^1-weighted, Δk = 3.8–9.2 Å^{-1}); (B) imaginary part and magnitude of Fourier transform of the experimental EXAFS (solid line) and sum of the calculated Ir–Ir + Ir–O_S + Ir–O_I contributions (dotted line) (k^1-weighted, Δk = 3.8–9.2 Å^{-1}); (C) normalized EXAFS function (solid line) and sum of the calculated Ir–Ir + Ir–O_S + Ir–O_I contributions (dotted line) (k^3-weighted, Δk = 3.8–9.2 Å^{-1}); (D) imaginary part and magnitude of Fourier transform of the experimental EXAFS (solid line) and sum of the calculated Ir–Ir + Ir–O_S + Ir–O_I contributions (dotted line) (k^3-weighted, Δk = 3.8–9.2 Å^{-1}).

both in k space and in r space, are shown in Figs. 5A–5D. The residual spectra determined by subtracting the Ir–Ir or the two Ir–O contributions from the raw data are shown in Figs. 6A and 6B, respectively.

Multiple shell fitting of the Fourier-filtered EXAFS spectrum (k^2-weighted, Δk: 3.67–11.62 Å^{-1}; Δr: 1.730–4.201 Å) of Ir/KLTL reduced at 500°C also identified three contributions (Table 2): an Ir–Ir contribution at 2.70 Å with a coordination number of 4.3 (indicating ca. 6 Ir atoms/cluster), an Ir–O contribution at 2.09 Å with a coordination number of 0.7, and a second Ir–O contribution at 2.67 Å with a coordination number of 1.2. The number of parameters used to fit the data is 12, with 13 degrees of freedom. The data (not shown) are similar to those shown for the sample treated in H_2 at 300°C.

Catalyst Performance

n-Hexane conversions less than about 10% were approximately differential. The reaction products were benzene, methylcyclopentane, 3-methylpentane, 2-methylpentane, 1-hexene, 2-hexene, 3-hexene, cyclohexane, cyclohexene, and C_{1-5} hydrocarbons. The turnover frequency (TOF), based on an Ir dispersion of unity, was about 0.12 s^{-1} at 400°C. For comparison, the TOF for Pt/KLTL zeolite at 420°C has been reported to be approximately 2 s^{-1} (7).

The product selectivity is given in Table 3. Benzene selectivity is defined as the fraction of *n*-hexane converted to benzene divided by the total conversion of *n*-hexane. Because hexane isomers (methylcyclopentane, 2-methylpentane, and 3-methylpentane), C_6 olefins, cyclohexane, and cyclohexene can also react to form benzene, a second (conventional) definition of benzene se-

TABLE 2

EXAFS Results Characterizing the KLTL Zeolite-Supported Iridium Clusters Prepared by the KLTL Zeolite with $[Ir(NH_3)_5Cl]Cl_2$ Followed by Flowing H_2 at 500°C and 1 atm for 1 h

Shell	N	R (Å)	$\Delta\sigma^2$ (Å^2)	ΔE_0 (eV)	EXAFS reference
Ir–Ir	4.2	2.70	0.0022	0.68	Pt–Pt
Ir–O_S	0.7	2.09	0.0085	7.05	Pt–O
Ir–O_I	1.2	2.67	0.0085	−6.50	Pt–O

Note. Notation as in Table 1. Estimated precision: N, ± 20% (Ir–$O_{support}$, ± 30%); R, ± 2% (Ir–Ir, ± 1%); $\Delta\sigma^2$, ± 30%; ΔE_0, ± 10%.

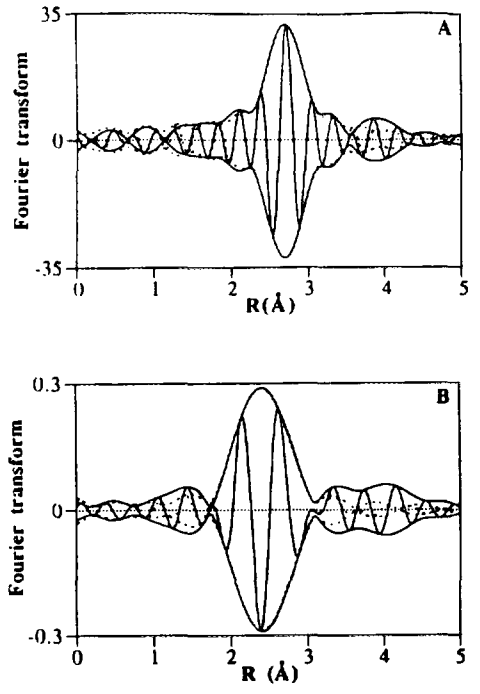

FIG. 6. Results of EXAFS analysis obtained with the best calculated coordination parameters characterizing KLTL zeolite-supported Ir clusters prepared by treatment of a KLTL zeolite prepared from $[Ir(NH_3)_5Cl]Cl_2$ treated at 300°C in flowing H_2 for 1 h. (A) Residual spectrum illustrating the EXAFS contributions characterizing the Ir–Ir interaction: imaginary part and magnitude of Fourier transform (k^3-weighted, Δk = 3.8–9.1 Å^{-1}) of raw data minus sum of the calculated Ir–O_S + Ir–O_I EXAFS (solid line) and calculated Ir–Ir EXAFS (dashed line) (Pt–Pt phase and amplitude corrected); (B) residual spectrum illustrating the EXAFS contributions characterizing the Ir–$O_{support}$ interaction: imaginary part and magnitude of Fourier transform (k^1-weighted, Δk = 3.8–9.1 Å^{-1}) of raw data minus EXAFS calculated for Ir–Ir (solid line) and sum of the calculated Ir–O_S + Ir–O_I EXAFS (dashed line) (Pt–O phase and amplitude corrected).

lectivity is also used to account for the irreversible loss of C_6 hydrocarbons by hydrogenolysis. This selectivity, referred to as the ultimate benzene selectivity, is the ratio of the *n*-hexane converted to benzene divided by the *n*-hexane converted to benzene and light (C_{1-5}) hydrocarbons. Finally, the ring closure selectivity is defined as the mass ratio of 1–6 ring closure products (the sum of benzene, cyclohexane, and cyclohexene) to 1–5 ring closure products (the sum of methylcyclopentane, 2-methylpentane, and 3-methylpentane).

Under the reaction conditions, approximately 40% of the products were olefins formed from dehydrogenation of *n*-hexane. An additional 30–40% of the *n*-hexane was converted into C_1–C_5 hydrocarbons by hydrogenolysis of *n*-hexane. Approximately 15% of the *n*-hexane was converted into benzene, and the remaining 10% of the products (methylcyclopentane, 2-methylpentane, and 3-methylpentane) resulted from 1–5 ring closure of *n*-hexane. The ultimate benzene selectivity was approximately 0.4 and was similar to the values reported briefly for Ir/KLTL (30, 31) and other Ir catalysts on nonacidic supports, e.g., Ir/SiO_2 (30) and Ir/MgO (31). The ring closure ratios (1–6/1–5) were 1.0, 1.4, and 2.6 at 400, 440, and 480°C, respectively, and were similar to the value observed for Pt/KLTL catalyst (4, 7, 31). For nonacidic Pt catalysts, ring closure ratios greater than 1.0 were observed only when the support was KLTL zeolite, whereas ring closure ratios of approximately 0.5 were observed for all other zeolite and amorphous catalysts (32).

DISCUSSION

Catalyst Structure

The results obtained by TPR, hydrogen chemisorption, infrared spectroscopy of adsorbed CO, TEM, and EXAFS spectroscopy are all consistent with the conclusion that the Ir^{3+} ions introduced into the zeolite were reduced to give small metal clusters at temperatures greater than 300°C. After reduction at 300°C, the first-shell Ir–Ir coordination number of 3.2 indicates that the average Ir clus-

TABLE 3

Selectivities in *n*-Hexane Conversion Catalyzed by Ir/KLTL Zeolite[a]

Reaction temperature (°C)	C_1	C_2–C_5	*i*–C_6^b	*i*–$C_6^=$	Benzene	Ultimate benzene	1–6/1–5 ring closure ratio
400[c]	0.23	0.31	0.12	0.22	0.12	0.18	1.0
440[d]	0.17	0.16	0.09	0.45	0.13	0.39	1.4
480[e]	0.29	0.09	0.06	0.39	0.16	0.42	2.6

[a] 1 atm total pressure, 76 Torr *n*-hexane partial pressure, H_2/*n*-hexane = 6.
[b] *i*-C_6 is the sum of methylcyclopentane, 2-methylpentane, and 3-methylpentane.
[c] *n*-Hexane conversion was 6.7% after 10 h.
[d] *n*-Hexane conversion was 6.2% after 10 h.
[e] *n*-Hexane conversion was 7.9% after 10 h.

ter nuclearity was about four atoms, corresponding to a diameter of about 6 Å. Reduction of Ir/KLTL at 500°C increased the average cluster size slightly to about six atoms/cluster (N = 4.3), corresponding to an average diameter of about 8 Å. After reduction at each temperature, the clusters were small enough to reside within the channels of LTL zeolite.

The Ir–Ir bond distance of 2.70 Å in the 4- to 6-atom Ir/KLTL clusters is the same as that for bulk Ir metal and other supported Ir catalysts, e.g., Ir clusters on alumina (33), silica (33), and magnesia (34). For example, in Ir/SiO_2, with an average Ir particle nuclearity of about 100 atoms, an Ir–Ir coordination number of 8.5, and an approximate particle size of 20 Å, the Ir–Ir bond distance was 2.70 Å (33). However, the Ir–Ir bond distance was found to be 2.64 Å for small Ir clusters (N = 5.5) on alumina, approximately 0.06 Å shorter than the bulk bond distance (35). The contraction of the metal–metal bond distance, however, was determined for a sample in the absence of chemisorbed hydrogen. In contrast, the EXAFS measurements of the catalysts reported here were made for samples in hydrogen. Similar results for the metal–metal bond distances in small Pt clusters have been reported; i.e., bulk metallic bond distances are observed for samples in the presence of chemisorbed hydrogen (36), whereas a contraction of about 0.1 Å in the bond distance has been observed for samples under vacuum (37).

In the highly dispersed Ir/KLTL zeolite catalysts, nearly all the Ir atoms are in contact with the support. Two Ir–O EXAFS contributions were observed for each sample (Tables 2 and 3). The shorter Ir–O distance is approximately equal to the sum of the covalent radii and is characteristic of metal atoms in contact with oxygen ions of the support (38). Similar metal–oxygen distances have been observed for Ir/Al_2O_3 (33, 35), Ir/MgO (33), Rh/MgO (33), and Pt/zeolite (36) catalysts. The longer Ir–O distance (2.67 Å) is significantly greater than the sum of the covalent radii of Ir and O, and it has been proposed that hydrogen atoms, similar in nature to chemisorbed hydrogen, reside between the support and the metal particles, leading to the long metal–oxygen distance (36, 38). A longer Pt–O distance (2.7 Å) was observed for supported Pt catalysts after low-temperature reduction (at 300°C), whereas a shorter Pt–O distance (2.2 Å) was present after high-temperature reduction (500°C) (36). The presence of the longer metal–oxygen distance after reduction at 500°C in the Ir/KLTL zeolite indicates that the long Ir–O distance is more thermally stable than the long Pt–O distance and is consistent with the higher hydrogen chemisorption capacity of Ir relative to Pt.

The infrared bands of linearly adsorbed CO in Ir/KLTL zerolite are in the frequency range of other zerovalent and anionic iridium carbonyl compounds (39–41) and supported catalysts (42–44), but the spectra of these various samples are different enough from each other that no strong structural conclusions emerge from the infrared spectra presented here.

The infrared spectrum of adsorbed CO on Ir/KLTL zeolite is also similar to that of CO terminally adsorbed on Pt/KLTL (11, 12, 32, 45, 46) and Pd/KLTL zeolites (32), for which several broad overlapping absorption bands occur between about 1950 and 2100 cm^{-1}. The low-frequency CO absorption bands for terminal CO on zeolite-supported and amorphous metal-oxide-supported Pt catalysts, at about 1950 cm^{-1}, are observed only when the supports are alkaline. These bands are thought to result from CO adsorbed on electron-rich Pt clusters interacting with basic metal oxide supports (11, 12, 15). The linear CO bands in the infrared spectra of Pt/KLTL zeolite were observed to shift to lower frequency as the catalyst was dried at higher temperatures (46). It was concluded that at low temperature adsorbed water on the K^+ ions disrupts the ion–dipole interaction, increasing the CO absorption frequency. A similar shift to lower frequency in the linear CO absorption bands is observed for CO adsorbed on Ir/KLTL zeolite at 50°C. The infrared spectra of Ir/KLTL zeolite therefore indicate that the zeolite is nonacidic, or slightly basic (consistent with the elemental analysis), with K^+ ions near the iridium clusters. Although the K^+ ions were sufficiently close to the Ir clusters to affect the frequency of the terminally bonded CO, the K^+ ions were not detected by EXAFS spectroscopy.

Implications for Catalysis

The size and steric and electronic environment of the Ir clusters in the Ir/KLTL catalysts of this investigation are almost identical to those of well-prepared Pt/KLTL naphtha reforming catalysts (23, 47). Although the Ir/KLTL support is nonacidic and *n*-hexane was converted into benzene by a mono-functional pathway, the hydrogenolysis selectivity of the Ir-containing catalysts was found to be high and the *n*-hexane aromatization selectivity poor, as is typical of other Ir catalysts, e.g., Ir/SiO_2 (30) and Ir/MgO (31). We infer that the combination of cluster size, electronic modification of the Ir by the support, and the steric environment near the metal clusters was not sufficient to suppress the high intrinsic hydrogenolysis selectivity of Ir. Thus, by comparison of these results with the results for Pt/KLTL zeolite, we infer that two criteria are critical for obtaining a selective aromatization catalyst: a nonacidic support (1, 8, 19) and a metal with low hydrogenolysis selectivity.

The excellent performance of Pt/KLTL zeolite catalysts implies that, although there are many potential cata-

lysts consisting of Pt on nonacidic supports, the structure of the support is important in providing some small improvements in selectivity, activity, and aromatization process economics. In Pt/KLTL catalysts, the hydrogenolysis activity is suppressed by addition of alkali (14, 47), which has been shown by infrared (11, 12, 15) and X-ray photoelectron spectroscopies (15) to increase the electron density on the metal clusters. The hydrogenolysis selectivity is also cluster size dependent, decreasing with decreasing cluster size (8). Furthermore, the specific pore geometry of the LTL zeolite increases the selectivity for 1–6 ring closure relative to 1–5 ring closure. This has an indirect effect on the hydrogenolysis selectivity, which becomes important at high conversion. For example, catalysts with a high 1–5 ring closure selectivity produce high yields of methylcyclopentane, 2-methylpentane, and 3-methylpentane. Before these can back-react to give benzene, they must first be converted into *n*-hexane through the methylcyclopentane intermediate. Each of the 1–5 ring closure products is also subject to hydrogenolysis. The higher the selectivity to 1–5 ring closure, therefore, the higher the hydrogenolysis selectivity in the limit as all the hexanes are converted into benzene, i.e., at high conversion. Thus, while there are many potential nonacidic naphtha aromatization catalysts, the most active and selective have small Pt clusters located within the pores of zeolite LTL with alkali contents adjusted to give the lowest hydrogenolysis selectivity while maintaining high aromatization activity.

CONCLUSIONS

Ir clusters in zeolite KLTL, consisting of four to six atoms on average, with sizes of about 6–8 Å, were prepared by reduction of $[Ir(NH_3)_5Cl]Cl_2$ in the zeolite in H_2 at temperatures $\geq$ 300°C. The clusters are sufficiently small to reside within the pores of the zeolite. EXAFS structural analysis indicates that there are two Ir–O distances, about 2.1 and 2.7 Å. The shorter distance is approximately the sum of the covalent radii of Ir and O. The longer distance has been suggested to result from chemisorbed hydrogen located between the Ir atoms and the oxygen ions of the support surface. The long Ir–O distance is thermally more stable that that observed in similar Pt/KLTL catalysts. The low-frequency infrared CO absorption bands characteristic of terminal CO suggest that the support environment is slightly basic and that the Ir clusters are electron rich relative to the bulk metal. Notwithstanding the small cluster size, the basic support environment, and the specific geometry of the LTL zeolite pore structure, the catalytic performance is similar to that of other Ir catalysts, with a poor selectivity for aromatization and a high selectivity for hydrogenolysis. Selective naphtha aromatization catalysts therefore require both a nonacidic support and a metal with a low hydrogenolysis activity, like Pt. Further improvements in the catalyst's aromatization selectivity result from reduction of the hydrogenolysis selectivity by optimization of the support alkalinity, cluster size, and steric environment.

ACKNOWLEDGMENTS

We thank N. Verbrüggen and Professor H. Knözinger of the University of Munich, where the TPR experiments were performed, J. B. Hall of Amoco Corporation Analytical Services for the transmission electron micrographs, and Professor D. C. Koningsberger of Utrecht University for providing the EXAFS analysis software. The research was supported by the U.S. Department of Energy, Office of Energy Research, Office of Basic Energy Sciences (Contract FG02-87ER13790). We also acknowledge the U.S. Department of Energy, Division of Materials Science, under Contract DE-FG05-89ER45384 for its role in the operation and development of Beamline X-11A at the National Synchrotron Light Source. The NSLS is supported by the Department of Energy, Division of Materials Science and Division of Chemical Sciences under Contract DE-AC02-76CH00016.

REFERENCES

1. Bernard, J. R., and Nury, J., U.S. Patent 4,104,320 to Elf France, 1978.
2. Bernard, J. R., *in* "Proceedings of the Fifth International Zeolite Conference" (L. V. C. Rees, Ed.), p. 686. Hayden, London, 1980.
3. Hughes, T. R., Buss, W. C., Tamm, P. W., and Jacobson, R. L., *in* "New Developments in Zeolite Science and Technology" (Y. Murakami, A. Iijima, and J. W. Ward., Eds.), p. 725, Studies in Surface Science and Catalysis, Vol. 28. Elsevier, Amsterdam, 1986.
4. Tamm, P. W., Mohr, D. H., and Wilson, C. R., *in* Studies in Surface Science and Catalysis, "Catalysis 1987" (J. W. Ward, Ed.), p. 335, Vol. 38, Elsevier, Amsterdam, 1988.
5. *Oil Gas J.* **190,** 19 (1992).
6. Rotman, D., *Chem. Week* **150,** 8 (1992).
7. Lane, G. S., Modica, F. S., and Miller, J. T., *J. Catal.* **129,** 145 (1991).
8. Mielczarski, E., Hong, S. B., Davis, R. J., and Davis, M. E., *J. Catal.* **134,** 359 (1992).
9. Larson, G., and Haller, G. L., *Catal. Lett.* **3,** 103 (1989).
10. Sharma, S. B., Miller, J. T., and Dumesic, J. A., *J. Catal.* **148,** 198 (1994).
11. Besoukhanova, C., Guidot, J., Barthomeuf, D., Breysse, M., and Bernard, J. R., *J. Chem. Soc. Faraday. Trans.* **77,** 1595 (1981).
12. Han, W.-H., Kooh, A. B., and Hicks, R. F., *Catal. Lett.* **18,** 193 (1993).
13. Han, W.-H., Kooh, A. B., and Hicks, R. F., *Catal. Lett.* **18,** 219 (1993).
14. Miller, J. T., Modica, F. S., Meyers, B. L., and Koningsberger, D. C., *Prepr. Div. Pet. Chem. Am. Chem. Soc.* **38,** 825 (1993).
15. Mojet, B. L., Kappers, M. J., Muijsers, J. C., Niemantsverdriet, J. W., Miller, J. T., Modica, F. S., and Koningsberger, D. C., *in* "Zeolites and Related Microporous Materials, State of the Art 1994" (J. Weitkamp, H. G. Karge, H. Pfeifer, and W. Hölderich, Eds.), p. 909, Studies in Surface Science and Catalysis, Vol. 84B, Elsevier, Amsterdam, 1994.
16. Tauster, S. J., and Steger, J. J., *J. Catal.* **125,** 387 (1990).
17. Alvarez, W. E., and Resasco, D. E., *Catal. Lett.* **8,** 53 (1991).
18. Derouane, E. G., and Vanderveken, D. J., *Appl. Catal.* **45,** L15 (1988).

19. Davis, R. J., and Derouane, E. G. *Nature (London)* **349,** 313 (1991).
20. Davis, R. J., and Derouane, E. G., *J. Catal.* **132,** 269 (1991).
21. Derouane, E. G., Julien-Lardoi, V., Davis, R. J., Blom, N., and Houjlund-Nielsen, P. E., *in* "New Frontiers in Catalysis" (L. Guczi, F. Solymosi, and P. Tetenyi, Eds.), p. 1031, Studies in Surface Science and Catalysis, Vol. 75, Elsevier, Amsterdam, 1993.
22. Iglesia, E., and Baumgartner, J. E., *in* "New Frontiers in Catalysis" (L. Guczi, F. Solymosi, and P. Tetenyi, Eds.), p. 993, Studies in Surface Science and Catalysis, Vol. 75, Elsevier, Amsterdam, 1993.
23. Vaarkamp, M., Grondelle, J. V., Miller, J. T., Sajkowski, D. J, Modica, F. S., Lane, G. S., Gates, B. C., and Koningsberger, D. C., *Catal. Lett.* **6,** 369 (1990).
24. Hong, S. B., Mielczarski, E., and Davis, M. E., *J. Catal.* **134,** 349 (1992).
25. Parry, R. W. (Ed.), "Inorganic Synthesis," Vol. XII. McGraw–Hill, New York, 1970.
26. Triantafillou, N. D., Ph.D. thesis, University of Delaware, 1993.
27. Koningsberger, D. C., *in* "Synchrotron Techniques in Interfacial Electrochemistry" (C. A. Melendres and A. Tadjeddine, Eds.), p. 181. Kluwer Academic, Dordrecht/Norwell, MA, 1994.
28. Kip, B. J., Duivenvoorden, F. B. M., Koningsberger, D. C., and Prins, R., *J. Catal.* **105,** 26 (1987).
29. Crozier, E. D., Rehr, J. J., and Ingalls, R., *in* "X-Ray Absorption: Principles, Applications, Techniques of EXAFS, SEXAFS, and XANES" (D. C. Koningsberger, and R. Prins, Eds.), p. 395. Wiley, New York, 1988.
30. Iglesia, E., and Baumgartner, J. E., *in* "Proceedings of the Ninth International Zeolite Conference" (R. von Ballmoos, J. B. Higgins, and M. M. J. Treacy, Eds.), p. 421. Butterworth–Heinemann, Boston, 1993.
31. Triantafillou, N. D., Miller, J. T., and Gates, B. C., *Prepr. Div. Pet. Chem. Am. Chem. Soc.* **38,** 812 (1993).
32. Lane, G. S., Miller, J. T., Modica, F. S., and Barr, M. K., *J. Catal.* **141,** 465 (1993).
33. von Zon, F. B. M., Ph.D. thesis, Eindhoven University, the Netherlands, 1988.
34. von Zon, F. B. M., Maloney, S. D., Gates, B. C., and Koningsberger, D. C., *J. Am. Chem. Soc.* **115,** 10317 (1993).
35. Kampers, F. W. H., and Koningsberger, D. C., *Faraday Discuss. Chem. Soc.* **89,** 137 (1990).
36. Vaarkamp, M., Modica, F. S., Miller, J. T., and Koningsberger, D. C., *J. Catal.* **144,** 611 (1993).
37. Moraweck, B., Clugnet, G., and Renouprez, A. J., *Surf. Sci.* **81,** L631 (1979).
38. Koningsberger, D. C., and Gates, B. C., *Catal. Lett.* **14,** 271 (1992).
39. Chini, P., Ciani, G., Garlaschelli, L., Manassero, M., Martinengo, S., and Sironi, A., *J. Organomet. Chem.* **152,** C35 (1978).
40. Bau, R., Chiang, M. Y., Wei, C.-Y., Garlaschelli, L., Martinengo, S., and Koetzle, T. F., *Inorg. Chem.* **23,** 4758 (1984).
41. Psaro, R., Dossi, C., Fusi, A., Della Pergola, R., and Garlaschelli, L., *J. Chem. Soc. Faraday Trans.* **88,** 369 (1992).
42. Maloney, S. D., Kelley, M. J., Koningsberger, D. C., and Gates, B. C., *J. Phys. Chem.* **95,** 9406 (1991).
43. McVicker, G. B., Baker, R. T. K., Garten, R. L., and Kugler, E. L., *J. Catal.* **65,** 207 (1980).
44. Xiao, F.-S., Xu, Z., Alexeev, O., and Gates, B. C., *J. Phys. Chem.* **99,** 1548 (1995).
45. Kustov, L. M., Ostgard, D., and Sachtler, W. M. H., *Catal. Lett.* **9,** 121 (1991).
46. Kappers, M. J., Vaarkamp, M., Miller, J. T., Modica, F. S., Barr, M. K., van der Maas, J. H., and Koningsberger, D. C., *Catal. Lett.* **21,** 235 (1993).
47. McVicker, G. B., Kao, J. L., Ziemiak, J. J., Gates, W. E., Robbins, J. L., Treacy, M. M. J., Rice, S. B., Vanderspurt, T. H., Cross, V. R., and Ghosh, A. K., *J. Catal.* **139,** 48 (1993).